

Terahertz Quantum Hall Effect in a Topological Insulator

A. M. Shuvaev,¹ G. V. Astakhov,² G. Tkachov,³ C. Brüne,⁴ H. Buhmann,⁴ L. W. Molenkamp,⁴ and A. Pimenov¹

¹*Institute of Solid State Physics, Vienna University of Technology, 1040 Vienna, Austria*

²*Physikalisches Institut (EP6), Universität Würzburg, 97074 Würzburg, Germany*

³*Institut für Theoretische Physik und Astronomie,
Universität Würzburg, 97074 Würzburg, Germany*

⁴*Physikalisches Institut (EP3), Universität Würzburg, 97074 Würzburg, Germany*

(Dated: August 7, 2012)

Using THz spectroscopy in external magnetic fields we investigate the low-temperature charge dynamics of strained HgTe, a three dimensional topological insulator. From the Faraday rotation angle and ellipticity a complete characterization of the charge carriers is obtained, including the 2D density, the scattering rate and the Fermi velocity. The obtained value of the Fermi velocity provides further evidence for the Dirac character of the carriers in the sample. In resonator experiments, we observe quantum Hall oscillations at THz frequencies. The 2D density estimated from the period of these oscillations agrees well with direct transport experiments on the topological surface state. Our findings open new avenues for the studies of the finite-frequency quantum Hall effect in topological insulators.

Three dimensional topological insulators [1, 2] have attracted much interest recently, as they exhibit a number of unusual and non-trivial properties, such as protected conducting states on the surfaces of the sample. Unusual electrodynamics, such as a universal Faraday effect and an anomalous Kerr rotation have been predicted [3–6] for these surface states, their observation is still outstanding. We showed recently that strained HgTe, where the strain lifts the light-hole–heavy-hole degeneracy that normally is present in bulk HgTe, is a very promising 3D topological insulator [7]. This is because at low temperatures parasitic effects due to bulk carriers are practically absent. In static transport experiments a strained 70 nm thick HgTe layer [7] exhibits a quantum Hall effect (QHE), yielding direct evidence that the charge carriers in these layers are confined to the topological two dimensional (2D) surface states of the material. These findings are further corroborated by recent Faraday rotation data [8] in a similar layer, which have been obtained using a terahertz time-domain technique.

In this work, we present the results of low temperature terahertz Faraday cw transmission experiments on another strained HgTe film. The carrier density, Fermi velocity and the scattering rate can be reliably determined from these data. In particular, we obtain the Fermi velocity $v_F = 0.52 \cdot 10^6$ m/s, which is in excellent agreement with the Faraday rotation experiments [8] and the dc Shubnikov-de Haas measurements [7] on 70-nm-thick strained HgTe films as well as with band-structure calculations for the surface states in 3D topological insulators (see e.g. Ref. [9]). In the same sample we observe quantum Hall-induced oscillations at terahertz frequencies, providing further evidence for the 2D character of the conductivity. In the case of topological insulators, no finite frequency QHE has been reported up to now.

The sample studied in this work is a coherently strained 52-nm-thick nominally undoped HgTe layer,

grown by molecular beam epitaxy on an insulating CdTe substrate [10]. Transmittance experiments at terahertz frequencies ($100 \text{ GHz} < \nu < 800 \text{ GHz}$) have been carried out in a Mach-Zehnder interferometer arrangement [11, 12] which allows measurement of the amplitude and phase shift of the electromagnetic radiation in a geometry with controlled polarization. Using wire grid polarizers, the complex transmission coefficient can be measured both in parallel and crossed polarizers geometry. Static magnetic fields, up to 8 Tesla, have been applied to the sample using a split-coil superconducting magnet.

To interpret the experimental data we use the ac conductivity tensor $\hat{\sigma}(\omega)$ obtained in the classical (Drude) limit from the Kubo conductivity of topological surface states (see e.g. Ref. [4]). The diagonal, $\sigma_{xx}(\omega)$, and Hall, $\sigma_{xy}(\omega)$, components of the conductivity tensor as functions of THz frequency ω can be written as:

$$\sigma_{xx}(\omega) = \sigma_{yy}(\omega) = \frac{1 - i\omega\tau}{(1 - i\omega\tau)^2 + (\Omega_c\tau)^2} \sigma_0, \quad (1)$$

$$\sigma_{xy}(\omega) = -\sigma_{yx}(\omega) = \frac{\Omega_c\tau}{(1 - i\omega\tau)^2 + (\Omega_c\tau)^2} \sigma_0. \quad (2)$$

Here, $\Omega_c = eBv_F/\hbar k_F$ is the cyclotron frequency, σ_0 is the dc conductivity, B is the magnetic field, v_F , k_F , e , and τ are the Fermi velocity, Fermi wave-number, charge, and scattering time of the carriers, respectively. For the Dirac spin-helical surface states the Fermi wave-number depends on the 2D carrier density, n_{2D} , through relation $k_F = \sqrt{4\pi n_{2D}}$, with no spin degeneracy.

The transmission spectra can then be calculated using a transfer matrix formalism [13–15] which takes multiple reflection within the substrate into account. The electrodynamic properties of the CdTe substrate have been obtained in a separate experiment on a bare substrate. Further details of the fitting procedure can be found in the Supplementary information to Ref. [15]. Neglecting any

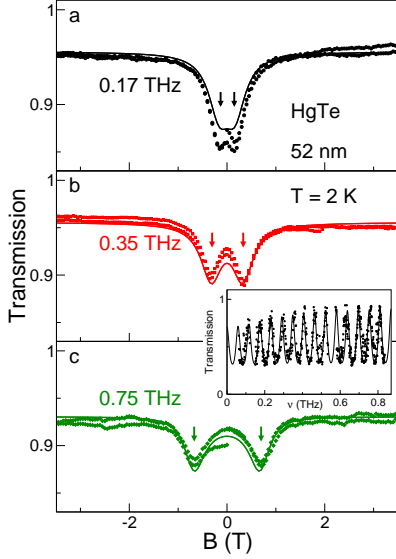


FIG. 1: *Magnetic field dependence of the transmission in strained HgTe.* (a-c) Transmission amplitude in parallel polarizers (t_p) geometry, showing cyclotron resonance at the positions indicated by the arrows. The frequency of the experiments is indicated in the panels. The inset shows the frequency dependent transmittance in zero external magnetic field, $|t_p(B=0)|^2$. Symbols: experiment, solid lines: simultaneous fit of all data with the Drude model as described in the text.

substrate effects, the complex transmission coefficients in parallel (t_p) and crossed (t_c) polarizers geometry can be written as:

$$t_p = \frac{4 + 2\Sigma_{xx}}{4 + 4\Sigma_{xx} + \Sigma_{xx}^2 + \Sigma_{xy}^2}, \quad (3)$$

$$t_c = \frac{2\Sigma_{xy}}{4 + 4\Sigma_{xx} + \Sigma_{xx}^2 + \Sigma_{xy}^2}. \quad (4)$$

Here Σ_{xx} and Σ_{xy} are effective dimensionless 2D conductivities, defined as: $\Sigma_{xx} = \sigma_{xx}dZ_0$ and $\Sigma_{xy} = \sigma_{xy}dZ_0$ with the HgTe film thickness $d = 52$ nm and the vacuum impedance $Z_0 \approx 377 \Omega$. In order to self-consistently obtain the parameters of the quasiparticles, the field-dependent complex transmission $t_p(B)$ and $t_c(B)$ for $\nu = 0.17$ THz, 0.35 THz and 0.75 THz and the zero-field transmittance spectra $|t_c(\omega)|^2$ have been fitted simultaneously.

The inset in Fig. 1 shows the transmittance spectrum of the HgTe film at zero magnetic field. The characteristic oscillations in the spectrum, with a period of about 58 GHz, are due to Fabry-Pérot type interferences within the CdTe substrate. The absolute transmittance in the interference maxima is close to 95%, which reflects the low effective conductance of our HgTe film, $\Sigma_{xx} \ll 1$. At low frequencies, the maximum transmittance decreases and approaches $|t_p|^2 \simeq 0.7$ in the zero frequency limit. Such a behavior is typical for Drude carriers with a scattering rate in the frequency region of the experiment.

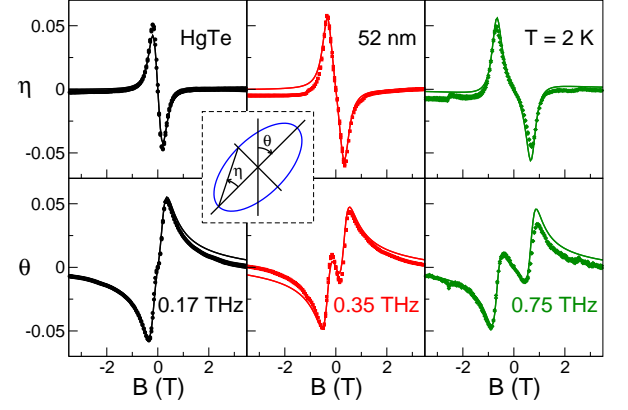


FIG. 2: *Complex Faraday angle $\theta + i\eta$ in HgTe.* Bottom panels: Faraday rotation, top panels: ellipticity for the same frequencies as in Fig. 1. The inset sketches the definitions of the Faraday rotation θ and ellipticity η . Symbols: experiment, solid lines: simultaneous fit of all data with the Drude model as described in the text. Angular units are radians.

Indeed, the solid line in the transmission spectra represents a Drude fit with the parameters given in the first row of Tab. I.

From the fits we obtain the Fermi velocity $v_F = 0.52 \cdot 10^6$ m/s. This value is very close both to $v_F = (0.51 \div 0.58) \cdot 10^6$ m/s as determined in the Faraday rotation experiments on a 70-nm-thick strained HgTe film [8] and to $v_F = 0.42 \cdot 10^6$ m/s as extracted from dc Shubnikov-de Haas measurements on a patterned 70-nm-thick strained HgTe layer [7]. The obtained value of the Fermi velocity is also in very good agreement with the band-structure-theory result $v_F = 0.51 \cdot 10^6$ m/s for the linear (Dirac) part of the surface-state spectrum in topological insulators (see e.g. Ref. [9]). As an additional check of the 2D surface carrier dynamics in our sample, we have analyzed the terahertz transmission data of Ref. [15] for a 70-nm-thick strained HgTe film at high temperature $T = 200$ K and for a bulk (1000-nm-thick) unstrained HgTe sample. In both cases, the electrodynamics is governed by massive bulk carriers, for which the values of v_F turn out to be much larger than the Dirac surface-state velocity, i.e., $v_F \approx 0.5 \cdot 10^6$ m/s (Tab. I).

Figure 1 shows the magnetic field dependent transmittance of the HgTe film in Faraday geometry and for parallel orientation of polarizer and analyzer. According to Eq. (3), the transmittance in parallel polarizers (t_p) depends mainly on Σ_{xx} . For all three frequencies two clear minima in the transmitted signal are observed in the range below ± 1 T. The minima in $|t_p|$ roughly correspond to the cyclotron resonance energy and scale with magnetic field. This may be understood taking into account that in our case $\Sigma \ll 1$ and Eqs. (3,4) simplify to:

$$t_p \simeq 1 - \Sigma_{xx}/2; \quad t_c \simeq \Sigma_{xy}/2. \quad (5)$$

TABLE I: Drude parameters of the charge carriers in HgTe in strained and unstrained films. The data on 70 nm and 1000 nm film were partly given in Ref. [15].

| Sample | $T(K)$ | $n_{2D}(cm^{-2})$ | $v_F(ms^{-1})$ | $1/2\pi\tau$ (GHz) | $G_{2D} = \sigma_0 \cdot d$ (Ω^{-1}) |
|------------------------------|--------|----------------------|-------------------|--------------------|---|
| 52 nm (strained) [this work] | 2 | $1.08 \cdot 10^{11}$ | $0.52 \cdot 10^6$ | 250 | $7.6 \cdot 10^{-4}$ |
| 70 nm (strained) [15] | 4 | $4.8 \cdot 10^{10}$ | $0.38 \cdot 10^6$ | 210 | $4.3 \cdot 10^{-4}$ |
| | 200 | $1.5 \cdot 10^{12}$ | $1.63 \cdot 10^6$ | 360 | $5.3 \cdot 10^{-3}$ |
| 1000 nm (unstrained) [15] | 3 | $4.2 \cdot 10^{11}$ | $0.99 \cdot 10^6$ | 240 | $2.8 \cdot 10^{-3}$ |
| | 200 | $4.9 \cdot 10^{13}$ | $9.36 \cdot 10^6$ | 360 | $1.9 \cdot 10^{-1}$ |

In the limit $\omega\tau \gg 1$, Eq. (1) may be approximated by

$$\sigma_{xx} \simeq \frac{1 - i\omega\tau}{(\Omega_c^2 - \omega^2)\tau^2} \sigma_0, \quad (6)$$

which leads to a resonance like feature for $\Omega_c = \omega$. Thus, the positions and widths of the minima in Fig. 1 are directly connected with the parameter v_F/k_F and the scattering rate τ^{-1} of the charge carriers.

Figure 2 shows the complex Faraday angle $\theta + i\eta$ as obtained at the same frequencies as in Fig. 1. The polarization rotation θ and the ellipticity η are obtained from the transmission data using:

$$\tan(2\theta) = 2\Re(\chi)/(1 - |\chi|^2), \quad (7)$$

$$\sin(2\eta) = 2\Im(\chi)/(1 + |\chi|^2). \quad (8)$$

Here $\chi = t_c/t_p$ and the definitions of $\theta + i\eta$ are shown graphically in the inset to Fig. 2. A direct interpretation of the complex Faraday angle is in general not possible because of the interplay of σ_{xx} and σ_{xy} in the data.

In the low frequency limit, $\omega\tau \ll 1$ Eq. (2) simplifies to the static result $\sigma_{xy} = \Omega_c\tau\sigma_0/(1 + (\Omega_c\tau)^2)$. The last expression has a maximum at $\Omega_c(B) = \tau^{-1}$, which leads to maxima in t_c and θ at about the same field value. Therefore, the Faraday angle provides a direct and an independent way of obtaining the scattering rate $1/\tau$. The solid line in Fig. 2 are the fits which have been done simultaneously for all results presented above. In total, the parameters of the charge carriers have been obtained by simultaneously fitting ten data sets. The quite reasonable fit of all results proves that a single type of charge carriers dominates the electrodynamics in the range of frequencies and magnetic fields used in these experiments.

Very solid evidence for the two dimensional character of the carriers probed in the Faraday rotation experiments would be the observation of quantum Hall plateaus, similar to the observation of the QHE in [7]. However, the accuracy of the experiments shown above does not allow to observe the QHE. In order to solve this problem, we have performed further Faraday transmission experiments on the same sample, now using a resonator geometry as shown in the inset of Fig. 3.

In these experiments, the sample is placed in the middle of a Fabry-Pérot resonator defined by metallic

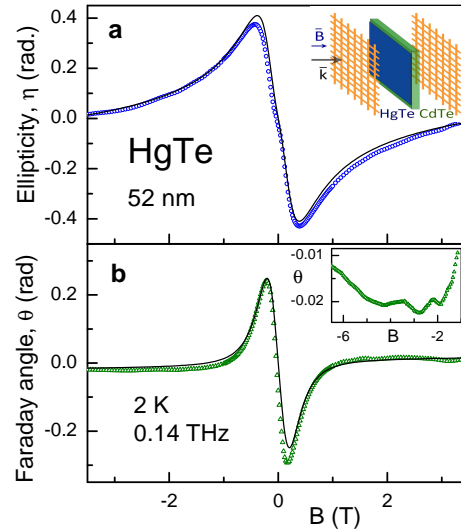


FIG. 3: Faraday rotation in HgTe within resonator geometry. (a) - Ellipticity, (b) - Faraday angle. Symbols - experiment, lines - fits according to Eqs. (1-4). Upper inset shows the experimental geometry within a Copper meshes resonator. Lower inset shows a magnified view of the Faraday angle demonstrating QHE oscillations.

meshes. We have utilized Cu meshes with a $200 \mu m$ period. The distance between adjacent maxima of the resonator is $\simeq 51$ GHz. In the frequency range between 100 and 200 GHz the quality factor of the loaded resonator is about $Q \sim 10$. This indicates that, effectively, the radiation passes about ten times through the sample before reaching the detector, which effectively increases the sensitivity to fine details by roughly the same value. As shown in Fig. 3, in the resonator experiments the field dependence of the Faraday rotation and the ellipticity appears qualitatively similar to that in Fig. 2. An exact calculation of the complex transmission coefficients within a resonator is complicated because of the increased number of parameters. Therefore, in this case we utilize the simple equations Eqs. (1)-(4) which neglect the effect of the substrate and the resonator completely. Nevertheless, as clearly seen in Fig. 3, the fits based on the simplified expressions reproduce the experimental results reasonably well. Fitting of the signals for parallel and crossed polarizers yields within experimental accu-

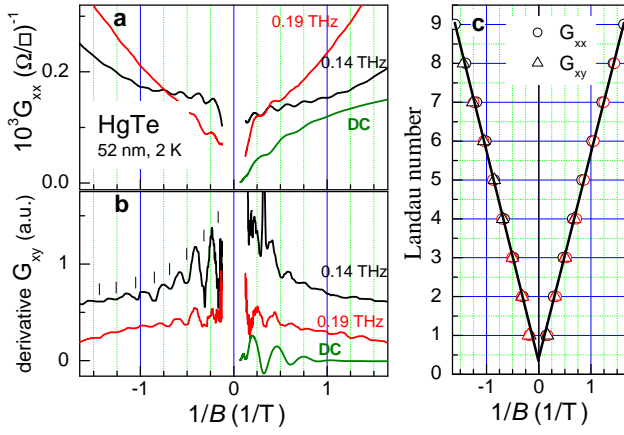


FIG. 4: *Terahertz quantum Hall effect in HgTe.* (a) Two dimensional conductance: G_{xx} , (b) derivative of G_{xy} (dG_{xy}/dB^{-1}). The data have been obtained within a resonator geometry and are plotted as a function of inverse magnetic field. The experimental data are shown as solid lines for frequencies as indicated. Dashes in the bottom panel marks the minima for negative magnetic fields. (c) Numbered positions of the minima in G_{xx} and in the derivative of G_{xy} for 0.14 THz and 0.19 THz. Straight lines yield interpolation to the origin.

racy the same parameters as in the experiments without a resonator. The only parameter which differs from the results without a resonator is the absolute value of the conductivity. This is of course expected, and results from multiple transmission in the resonator and the influence of the substrate.

The main advantage of the resonator experiments is a higher sensitivity to the details of the field-dependent transmission. In addition to an overall field dependence similar to that in Figs. 1 and 2, a tiny modulation of the signal can now be observed. To convert this modulation to a conventional presentation, we have inverted the transmittance curves into the 2D conductivity, using Eqs. (3 and 4). Because the absolute transmittance is not well-defined in the resonator experiments, we have scaled the absolute 2D conductance to agree with the data without a resonator. The final results expressed in form of the effective 2D conductance $G_{xx,xy} = \Sigma_{xx,xy}/Z_0$ are shown in Fig. 4.

Fig. 4a shows the real part of the two dimensional conductance G_{xx} as a function of inverse magnetic field. Clear oscillations in the conductance can be observed in this presentation. In general, the phenomenology of the QHE at terahertz frequencies is not well understood [16, 17]. Existing experiments are generally limited to frequencies below 100 GHz and they are analyzed using scaling exponents [16, 18]. In the resonator experiments, the field dependent oscillations can be observed both with parallel and crossed polarizers. Contrary to G_{xx} , the off-diagonal conductance G_{xy} shows a substantial field dependence even in high magnetic fields. Therefore, no

clear QHE signal can be directly detected in G_{xy} . In order to extract the QHE information from these data, we have plotted the derivative of the G_{xy} as a function of an inverse magnetic field (dG_{xy}/dB^{-1}) in Fig. 4b. The derivative has the advantage of being insensitive to any residual slowly varying signals, and, importantly, the expected steps in G_{xy} are transformed into the minima of the derivative. Finally, in order to analyze the quantum Hall effect, both the minima in G_{xx} and in the derivative of G_{xy} have been taken into account. In Fig. 4a,b the results at finite frequencies are compared with dc QHE on the same sample. The periodicity of the oscillations in the dc experiments is slightly different because of different carrier concentration at the sample surface, induced by exposure to photoresist and the presence of ohmic contacts.

The main results of the QHE experiments are represented in Fig. 4c demonstrating an approximate equidistant positioning of all minima (labeled by number N) in inverse magnetic fields B^{-1} with the period of $\Delta B^{-1} = 0.18 \text{ T}^{-1}$. This periodicity reflects the dependence of the number of the occupied Landau levels on B^{-1} . In a total, we detect the oscillations up to index number ± 10 ; also the first oscillations with the Landau level index ± 1 are clearly observed in the data. From the periodicity of these oscillations the effective 2D carrier density can be estimated according to the free electron expression $n_{2D} = e/(h\Delta B^{-1}) \simeq 1.4 \cdot 10^{11} \text{ cm}^{-2}$. This value agrees reasonably well with the density $n_{2D} = 1.08 \cdot 10^{11} \text{ cm}^{-2}$ obtained directly from fitting the transmittance and the Faraday rotation on the basis of the Drude model (Tab. I). Therefore, we may conclude that charge carriers which are responsible for the terahertz electrodynamics at low temperatures reveal 2D behavior. To further characterize the electron system in our sample we extrapolated the dependence $N(B^{-1})$ to the origin (see straight lines in Fig. 4c), which corresponds to the limit of very strong magnetic fields. At the origin we find a finite value $N \approx 1/2$ instead of $N = 0$ as would be the case for the conventional QHE. Previously, similar extrapolated values were reported for graphene (see e.g. Ref. [19]), zero-gap HgTe quantum wells [20] and strained 70 nm-thick HgTe films [7], i.e. for materials with 2D Dirac-like charge carriers encoding a nonzero Berry phase. We therefore believe that our terahertz QHE also indicates the 2D Dirac-like behavior.

In conclusion, we have analyzed the terahertz Faraday rotation in a strained HgTe film. From these data all relevant parameters of the charge carriers can be obtained. In addition, terahertz quantum Hall effect oscillations have been observed within the same experiment, which proved the two-dimensional character of the conductivity.

We thank E. M. Hankiewicz for valuable discussion. This work was supported by the by the German Research Foundation DFG (SPP 1285, FOR 1162) the joint

DFG-JST Forschergruppe on 'Topological Electronics', the ERC-AG project '3-TOP', and the Austrian Science Funds (I815-N16).

-
- [1] M. Z. Hasan and C. L. Kane. *Colloquium* : Topological insulators. *Rev. Mod. Phys.*, 82:3045–3067, Nov 2010.
 - [2] Xiao-Liang Qi, Taylor L. Hughes, and Shou-Cheng Zhang. Topological field theory of time-reversal invariant insulators. *Phys. Rev. B*, 78:195424, Nov 2008.
 - [3] Wang-Kong Tse and A. H. MacDonald. Giant magneto-optical kerr effect and universal faraday effect in thin-film topological insulators. *Phys. Rev. Lett.*, 105:057401, Jul 2010.
 - [4] W.-K. Tse and A. H. MacDonald. Magneto-optical faraday and kerr effects in topological insulator films and in other layered quantized hall systems. *Phys. Rev. B*, 84:205327, 2011.
 - [5] Joseph Maciejko, Xiao-Liang Qi, H. Dennis Drew, and Shou-Cheng Zhang. Topological quantization in units of the fine structure constant. *Phys. Rev. Lett.*, 105:166803, Oct 2010.
 - [6] G. Tkachov and E. M. Hankiewicz. Anomalous galvanomagnetism, cyclotron resonance, and microwave spectroscopy of topological insulators. *Phys. Rev. B*, 84:035405, Jul 2011.
 - [7] C. Brüne, C. X. Liu, E. G. Novik, E. M. Hankiewicz, H. Buhmann, Y. L. Chen, X. L. Qi, Z. X. Shen, S. C. Zhang, and L. W. Molenkamp. Quantum hall effect from the topological surface states of strained bulk hgte. *Phys. Rev. Lett.*, 106:126803, Mar 2011.
 - [8] Jason N. Hancock, J. L. M. van Mechelen, Alexey B. Kuzmenko, Dirk van der Marel, Christoph Brüne, Elena G. Novik, Georgy V. Astakhov, Hartmut Buhmann, and Laurens W. Molenkamp. Surface state charge dynamics of a high-mobility three-dimensional topological insulator. *Phys. Rev. Lett.*, 107:136803, Sep 2011.
 - [9] C.-X. Liu, X.-L. Qi, Zhang H. J., Xi Dai, Z. Fang, and S.-C. Zhang. Model hamiltonian for topological insulators. *Phys. Rev. B*, 82:045122, 2010.
 - [10] C. R. Becker, C. Brüne, M. Schäfer, A. Roth, H. Buhmann, and L. W. Molenkamp. The influence of interfaces and the modulation doping technique on the magnetotransport properties of hgte based quantum wells. *physica status solidi (c)*, 4(9):3382–3389, 2007.
 - [11] A. A. Volkov, Yu. G. Goncharov, G. V. Kozlov, S. P. Lebedev, and A. M. Prokhorov. Dielectric measurements in the submillimeter wavelength region. *Infrared Phys.*, 25(1-2):369, 1985.
 - [12] A. Pimenov, S. Tachos, T. Rudolf, A. Loidl, D. Schrupp, M. Sing, R. Claessen, and V. A. M. Brabers. Terahertz conductivity at the verwey transition in magnetite. *Phys. Rev. B*, 72(3):035131, Jul 2005.
 - [13] D. W. Berreman. Optics in stratified and anisotropic media - 4x4-matrix formulation. *J. Opt. Soc. Am.*, 62(4):502, 1972.
 - [14] A. M. Shuvaev, S. Engelbrecht, M. Wunderlich, A. Schneider, and A. Pimenov. Strong dynamic magnetoelectric coupling in metamaterial. *Eur. Phys. J. B*, 79:163–167, 2011. 10.1140/epjb/e2010-10493-1.
 - [15] A. M. Shuvaev, G. V. Astakhov, A. Pimenov, C. Brüne, H. Buhmann, and L. W. Molenkamp. Giant magneto-optical faraday effect in hgte thin films in the terahertz spectral range. *Phys. Rev. Lett.*, 106:107404, Mar 2011.
 - [16] F. Hohls, U. Zeitler, R. J. Haug, R. Meisels, K. Dybko, and F. Kuchar. Dynamical scaling of the quantum hall plateau transition. *Phys. Rev. Lett.*, 89:276801, Dec 2002.
 - [17] Y. Ikebe, T. Morimoto, R. Masutomi, T. Okamoto, H. Aoki, and R. Shimano. Optical hall effect in the integer quantum hall regime. *Phys. Rev. Lett.*, 104:256802, Jun 2010.
 - [18] S. L. Sondhi, S. M. Girvin, J. P. Carini, and D. Shahar. Continuous quantum phase transitions. *Rev. Mod. Phys.*, 69:315–333, Jan 1997.
 - [19] K. S. Novoselov, A. K. Geim, S. V. Morozov, D. Jiang, M. I. Katsnelson, I. V. Grigorieva, S. V. Dubonos, and A. A. Firsov. Two-dimensional gas of massless dirac fermions in graphene. *Nature (London)*, 438:197, 2005.
 - [20] B. Büttner, C. X. Liu, G. Tkachov, E. G. Novik, C. Brüne, H. Buhmann, E. M. Hankiewicz, P. Recher, B. Trauzettel, S. C. Zhang, and L. W. Molenkamp. Single valley dirac fermions in zero-gap hgte quantum wells. *Nature Physics*, 7(5):418–422, MAY 2011.